

Polaromechanics: photons, magnons and phonons in the triple strong-coupling regime

Rui-Chang Shen,¹ Jie Li,^{1,*} Yi-Ming Sun,¹ Wei-Jiang Wu,¹ Xuan Zuo,¹ Yi-Pu Wang,¹ Shi-Yao Zhu,^{1,2,3} and J. Q. You^{1,2,†}

¹Zhejiang Key Laboratory of Micro-Nano Quantum Chips and Quantum Control, School of Physics, and State Key Laboratory for Extreme Photonics and Instrumentation, Zhejiang University, Hangzhou 310027, China

²College of Optical Science and Engineering, Zhejiang University, Hangzhou 310027, China

³Hefei National Laboratory, Hefei 230088, China

Building hybrid quantum systems is a crucial step for realizing multifunctional quantum technologies, quantum information processing, and hybrid quantum networks. A functional hybrid quantum system requires strong coupling among its components. However, couplings between distinct physical systems are typically very weak. Experimental realization of strong coupling in a hybrid system remains a long-standing challenge, especially when it has multiple components and the components are of different nature. Here we demonstrate the realization of triple strong coupling in a novel *polaromechanical* hybrid system, where polaritons, formed by strongly coupled ferromagnetic magnons and microwave photons, are further strongly coupled to phonons. The corresponding polaromechanical normal-mode splitting is observed. A high polaromechanical cooperativity of 9.4×10^3 is achieved by significantly reducing the polariton decay rate via exploiting coherent perfect absorption. The quantum cooperativity much greater than unity is achievable if placing the system at low bath temperatures, which would enable various quantum applications. Our results pave the way towards coherent quantum control of photons, magnons and phonons, and are a crucial step for building functional hybrid quantum systems based on magnons.

Quantum information processing, quantum technologies, and the building of hybrid quantum networks require hybrid quantum systems (HQSs), which combine different physical systems with their individual strengths and complementary functionalities, to store, process, and transmit quantum information [1–4]. A prerequisite for realizing a functional HQS is the ability to exchange quantum states between its components with high fidelity, which requires strong coupling, where reversible energy exchange between interacting systems is faster than their energy dissipations to the environments. To date, strong coupling has been realized in a variety of quantum systems, such as atoms and optical photons [5], superconducting qubits and microwave photons [6], excitons and microcavity photons [7], among others. In terms of mechanical systems, promising components for HQSs given their ability to couple with various quantum systems and high quality factors, strong coupling has been achieved with optical or microwave photons [8–10], a superconducting qubit [11–15], a quantum dot [16], atomic spins [17], etc. This enables not only the function of a mechanical “quantum bus” for interfacing and

communicating between different quantum systems, but also the preparation and control of quantum states of mechanical oscillators, which has been a subject of long-standing interest [18].

Of particular interest is to build HQSs composed of more than two components, ranging from photons, atoms, and spins to superconducting and nanomechanical structures, especially when they are of different nature, where hybridization is maximized to integrate complementary functionalities. Over the past few years, collective spin excitations (magnons) in magnetic materials, e.g. yttrium iron garnet (YIG), have been demonstrated as possible building blocks for novel quantum technologies [19, 20], quantum information processing [21], quantum networks [22], and quantum computing [23]. Their unique feature is that they can coherently interact with a variety of quantum systems including microwave or optical photons, superconducting qubits, vibration phonons, etc [24–26]. However, couplings between excitations of distinct physical systems are typically very weak, and this is particularly the case when the excitation frequencies differ greatly [2]. Up to now, the realization of strong coupling among more than two physical systems remains challenging and an outstanding goal.

Here, we report an experimental realization of triple strong coupling in a HQS involving three different quanta, namely, ferromagnetic magnons, microwave photons, and long-lived phonons. Specifically, we realize strong coupling in a novel *polaromechanical* system (a new type of HQSs [27]), in which polaritons, hybrid quasiparticles formed due to the strong light-matter interaction [28], couple to vibration phonons. In the experiment, magnon polaritons (MPs) are formed by strongly coupled magnons and microwave cavity photons, and vibrational phonons are induced by the magnetostriction of a YIG sphere. The decay rate of the MP can be significantly reduced by operating the system at the conditions of coherent perfect absorption (CPA) [29–32], under which the microwave cavity mode achieves an effective gain [33]. By further operating the system at the (cavity) gain-(magnon) loss balance, the decay rate of the MP is reduced to nearly zero. This, together with the small mechanical damping rate, leads to the strong coupling between the mechanical mode and the driven MP, as witnessed by an evident normal-mode splitting (NMS) at the mechanical sideband. The normal modes of the system are then the hybridization of photons, magnons and phonons, implying that the system is in the triple strong-coupling regime. A remarkably high polaromechanical cooperativity $\sim 9.4 \times 10^3$ is accordingly achieved.

* jieli007@zju.edu.cn

† jqyou@zju.edu.cn

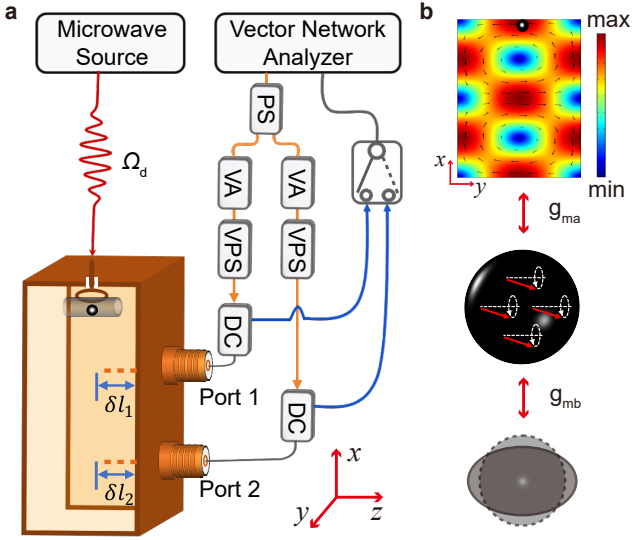


Fig. 1. Schematic diagram of the experimental setup. **a** The microwave signal generated by a vector network analyzer (VNA) is equally divided into two beams through a power splitter (PS). The amplitude and phase of each beam can be independently tuned by a variable attenuator (VA) and variable phase shifter (VPS). The two microwave fields are injected into the cavity after through two directional couplers (DCs) connected to the two ports, and the output fields are measured by the VNA after the DCs. The microwave cavity is a 3D oxygen-free copper cavity with dimensions of $60 \times 25 \times 6 \text{ mm}^3$, and a 0.25-mm-diameter YIG sphere is placed at the antinode of the magnetic field of the cavity TE_{102} mode. The YIG sphere is supported by a horizontal glass capillary and can move freely to reduce the mechanical damping. At the top of the cavity, a coil connected with a microwave source is used to directly drive the YIG sphere. Each cavity port is fixed with a SMA adaptor, and the length of the SMA adaptor's pin entering the cavity $\delta l_{1(2)}$ can be tuned. The external magnetic field B_0 (in the z direction) is applied to set the frequency of the magnon mode. The experiment is performed at room temperature. **b** Three interacting modes of the system, including a cavity mode, a magnon mode, and a vibration mode. At the top is the magnetic field distribution of the cavity TE_{102} mode.

Results

The polaromechanical system

The polaromechanical system is schematically shown in Fig. 1a, which consists of a 3D microwave cavity and a YIG sphere supporting both a magnon mode and a deformation vibration mode [34]. The magnon mode couples to the microwave cavity mode via the magnetic dipole interaction [35–37], and to the mechanical vibration mode via the magnetostrictive interaction [38–41] (Fig. 1b). The cavity TE_{102} mode has a resonance frequency $\omega_a/2\pi = 7.213 \text{ GHz}$ and a total decay rate κ_a , which is contributed by three dissipation channels, i.e., $\kappa_a = \kappa_{\text{int}} + \kappa_1 + \kappa_2$, with the intrinsic decay rate $\kappa_{\text{int}}/2\pi = 1.98 \text{ MHz}$, and the external decay rate $\kappa_{1(2)}$ due to the connection to the cavity port 1(2). To implement the CPA, $\kappa_{1(2)}$ is set to be tunable by adjusting the length $\delta l_{1(2)}$ of the SMA adaptor's pin into the cavity. The frequency of the magnon mode can be continuously adjusted by varying the external bias magnetic field B_0 via $\omega_m = \gamma B_0$, with the gyromagnetic ratio $\gamma/2\pi = 28 \text{ GHz/T}$. The magnon decay rate $\kappa_m/2\pi = 0.49 \text{ MHz}$, and the magnon-cavity coupling strength $g_{ma}/2\pi = 6.63 \text{ MHz}$. The magnon mode is driven by a mi-

crowave field loaded via a loop antenna, which further drives the mechanical mode through the magnomechanical coupling. In the experiment, we observe three mechanical modes with close resonance frequencies (see the Supplementary Information (SI) for details), and we focus on the mode of frequency $\omega_b/2\pi = 10.9565 \text{ MHz}$, which exhibits the strongest bare magnomechanical coupling rate $g_{mb}/2\pi = 1.40 \text{ mHz}$ and the lowest damping rate $\kappa_b/2\pi = 155 \text{ Hz}$.

Thanks to the high spin density of the YIG, the magnon mode and the cavity are strongly coupled, $g_{ma} > \kappa_a, \kappa_m$, leading to two hybridized MPs [35–37]. The corresponding frequencies ω_{\pm} and decay rates κ_{\pm} of the two polariton modes are given by $\omega_{\pm} - i\kappa_{\pm} = \frac{1}{2} [(\omega_a + \omega_m) - i(\kappa_a + \kappa_m) \pm \xi^{\frac{1}{2}}]$, where $\xi = 4g_{ma}^2 + [(\omega_a - \omega_m) - i(\kappa_a - \kappa_m)]^2$. The linearized Hamiltonian of the system in terms of two polariton modes reads (see SI)

$$H/\hbar = \omega_+ p_+^\dagger p_+ + \omega_- p_-^\dagger p_- + \omega_b b^\dagger b + (G_+ p_+^\dagger + G_+^* p_+) x + (G_- p_-^\dagger + G_-^* p_-) x, \quad (1)$$

where $p_+ = a \cos \theta + m \sin \theta$ and $p_- = -a \sin \theta + m \cos \theta$ denote the annihilation operators of the upper- and lower-branch polaritons, respectively, satisfying the bosonic commutation relation $[p_{\pm}, p_{\pm}^\dagger] = 1$, and $\theta = \frac{1}{2} \arctan\left(\frac{2g_{ma}}{\omega_a - \omega_m}\right)$ determines the proportion of the magnon (cavity) mode in the two polaritons; a , m , and b (a^\dagger , m^\dagger , and b^\dagger) are the annihilation (creation) operators of the cavity, magnon and mechanical modes, respectively, and $x = (b + b^\dagger)/\sqrt{2}$ denotes the mechanical displacement by magnetostriction; $G_{+(-)}$ is the effective coupling strength between the upper (lower)-branch polariton and the mechanical mode, and their expressions are

$$G_+ = \sqrt{2} g_{mb} M \sin \theta, \quad G_- = \sqrt{2} g_{mb} M \cos \theta, \quad (2)$$

with M being the steady-state average of the magnon mode. Equation (2) indicates that the polaromechanical coupling $G_{+(-)}$ can be significantly enhanced by strongly driving the magnon mode to have a large M . When the coupling rate exceeds the dissipation rates of the polariton and mechanical modes, i.e., $G_{+(-)} > \kappa_{+(-)}, \kappa_b$, the system enters the triple strong-coupling regime, in which the normal modes are the hybridization of photons, magnons and phonons. Previous experiments have demonstrated relatively weak couplings, i.e., G_{\pm} up to tens of kHz [34], due to the intrinsically small bare coupling $g_{mb} < 10 \text{ mHz}$, which is much smaller than the polariton decay rates $\kappa_{\pm} \sim 1 \text{ MHz}$ (limited by the magnon intrinsic loss). The enhancement of the coupling strength G_{\pm} by further increasing the drive power is restricted by strong nonlinear effects of the YIG sphere [41, 42]. Therefore, the triple strong coupling of the system is yet to be achieved.

Polariton decay rate reduction via CPA

A natural idea to achieve the polaromechanical strong coupling is to reduce the dissipation rate of the polariton mode. To this end, we exploit the CPA to achieve an effective gain of the cavity mode. This approach has been adopted to realize the exceptional point associated with the parity-time symmetry in cavity magnonics [33] and optical microcavities [32]. Under

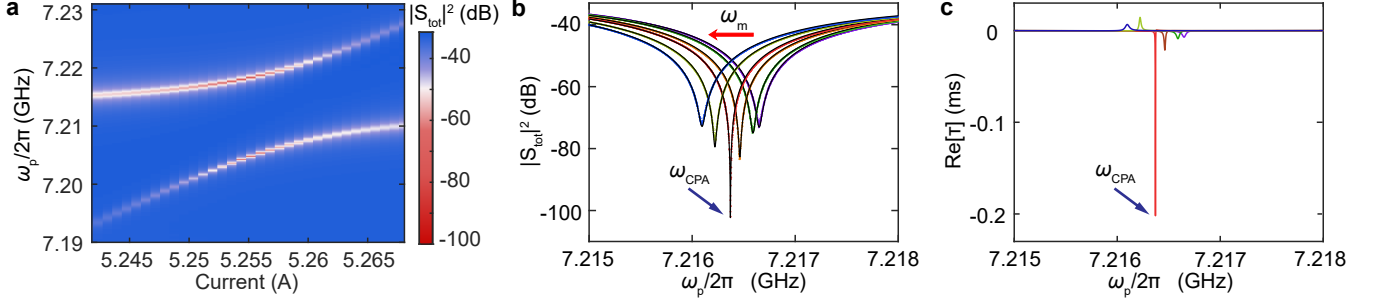


Fig. 2. Reduction of the polariton decay rate and characterization of the CPA. **a** Output spectrum of the CPA with $\kappa_1/2\pi = 1.22$ MHz, $\kappa_2/2\pi = 1.24$ MHz, $\Delta\phi = 0$, and $q \approx 1$. The output spectrum $|S_{\text{tot}}|^2 = |r_i + t_j|^2$ ($i \neq j = 1, 2$) contains the reflection (transmission) field of the input field loaded at port i (j). ω_p is the frequency of the input field. The frequency of the magnon mode is tuned by varying the bias magnetic field via adjusting the electromagnetic current. **b** Output spectra of the upper-branch polariton with different magnon frequencies. As the frequency of the polariton approaches the CPA frequency ω_{CPA} , via tuning the magnon frequency (red arrow indicates the direction), the polariton decay rate decreases manifesting as a rapid reduction of the output field. The smallest decay rate of the polariton is achieved at the CPA frequency. Black curves are fitting results. **c** The Wigner time delay $\text{Re}[\tau(\omega)]$ corresponding to the output spectra in **b**. The long time delay ~ 0.2 ms signifies the significantly reduced decay rate of the polariton at the CPA frequency.

the CPA conditions, the output field of the cavity $A_{1(2)}^{\text{out}} = 0$. The input-output relation $A_{1(2)}^{\text{out}} = \sqrt{2\kappa_{1(2)}}A - a_{1(2)}^{\text{in}}$ [43] thus leads to the input field $a_{1(2)}^{\text{in}} = \sqrt{2\kappa_{1(2)}}A$, which provides a gain for the cavity mode (see SI). The cavity mode is then compensated to be a gain mode with an effective gain rate [33]: $\kappa'_a \equiv \kappa_1 + \kappa_2 - \kappa_{\text{int}}$. The CPA requires that the cavity gain and the magnon loss are balanced, i.e., $\kappa'_a = \kappa_m$, for the resonant case of $\omega_m = \omega_a$, which leads to the vanishing of the polariton decay rates, i.e., $\kappa_{\pm} = \frac{-\kappa'_a + \kappa_m}{2} = 0$ (see SI for derivation). The significantly reduced polariton decay rates, together with the intrinsically small mechanical damping rate, offers the possibility to observe the polaromechanical strong coupling.

In the experiment, accurate realization of the gain-loss balance is vital to obtain vanishing polariton decay rates. To this end, we alter the length of the pins $\delta l_{1(2)}$ to vary $\kappa_{1(2)}$ in order to meet $\kappa'_a = \kappa_m$. Figure 2a shows the output spectrum with $\kappa_1/2\pi = 1.22$ MHz and $\kappa_2/2\pi = 1.24$ MHz. The two input fields are adjusted to have a zero phase difference $\Delta\phi = 0$ and a power ratio $q = \kappa_2/\kappa_1 \approx 1$ (see SI). The phase difference and power ratio are tuned via the VPS and VA connected to each port (Fig. 1a). As shown in Fig. 2a, when the frequency of the magnon mode approaches the cavity resonance, the output spectrum exhibits remarkable dips. Due to the monochromaticity of the CPA [29, 31, 44], the output spectrum is nearly zero at the CPA frequency ω_{CPA} . Consequently, we obtain the smallest symmetric decay rates of the two MPs $\kappa_{\pm}/2\pi = 7.75$ kHz, limited by the regulation precision.

To further reduce the decay rate of the polariton, we tune the magnon frequency by varying the bias magnetic field while keeping the cavity frequency fixed. This further reduces the decay rate of one polariton at the price of increasing that of the other (see SI for details). In this way, by red-shifting the magnon frequency we achieve the decay rate of the upper-branch polariton $\kappa_+/2\pi = 0.78$ kHz, corresponding to an output of -100.4 dB (Fig. 2b).

The significantly reduced polariton decay rate can be substantiated by calculating the Wigner time delay (WTD) [44, 45], which characterizes the trapped time of the input field in

the resonator (i.e., the MP). The CPA corresponds to the input field being infinitely trapped in the resonator, which can be translated into a diverging WTD. The exact CPA is unmeasurable in the experiment: one can only achieve nearly perfect absorption by improving the control accuracy. This corresponds to a finite WTD, which can be used to estimate the decay rate of the polariton. The WTD is defined as the real part of the complex-valued $\tau(\omega)$ [44, 45], i.e.,

$$\tau(\omega) = \frac{-i\psi_{\text{in}}^* S^*(\omega) \partial_{\omega} S(\omega) \psi_{\text{in}}}{\psi_{\text{in}}^* S^*(\omega) S(\omega) \psi_{\text{in}}}, \quad (3)$$

where $S(\omega)$ is the scattering matrix (see SI for details) and $\psi_{\text{in}} = (a_1^{\text{in}}, a_2^{\text{in}})^{\text{T}}$ is the vector of input fields. In Fig. 2c, we calculate the WTD associated with the output spectra in Fig. 2b. Note that there is a one-to-one correspondence between the spectra in Fig. 2b and the WTD in Fig. 2c at each frequency, and a phase transition of $\text{Re}[\tau]$ occurs at the singularity point, i.e., the exact CPA [44]. At the CPA frequency, we obtain a maximum WTD $|\text{Re}[\tau(\omega_{\text{CPA}})]| = 0.2$ ms, corresponding to the decay rate of the polariton $\kappa_+ = 1/\text{Re}[\tau(\omega_{\text{CPA}})] = 2\pi \times 0.79$ kHz. This agrees well with the value $\kappa_+/2\pi = 0.78$ kHz evaluated using the theory provided in the SI.

Polaromechanical normal-mode splitting

The coupling between the MPs and the mechanical mode essentially originates from the dispersive magnetostrictive (magnon-phonon) interaction, which leads to the linearized Hamiltonian in equation (1). It reveals that the interaction between each polariton and the mechanical mode is analogous to the linearized opto- [46] and magnomechanical [34] Hamiltonian. This promises similar polaromechanical backaction as the opto- and magnomechanical ones, such as mechanical cooling and amplification [34, 47]. Equation (2) indicates that the effective polaromechanical coupling G_{\pm} can be enhanced by increasing the magnon excitation number. In the experiment, we adopt a red-detuned microwave field to drive the upper-branch polariton and to keep the scattered mechanical sideband in resonance with the polariton (Fig. 3a). This enhances the magnomechanical anti-Stokes scattering, which

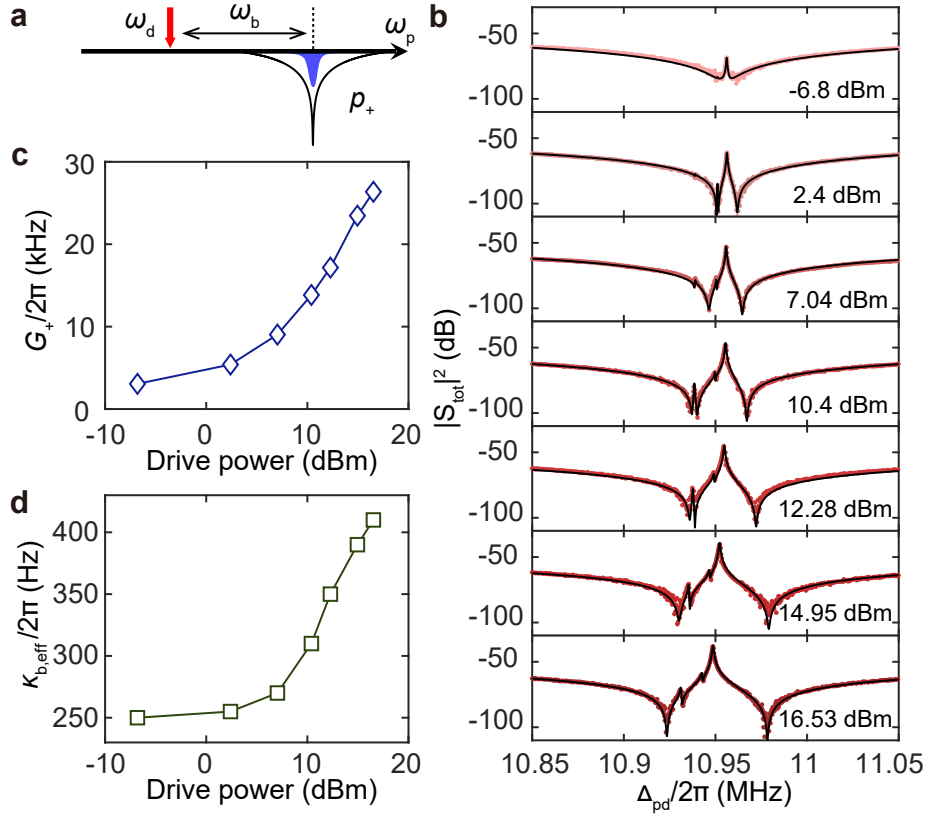


Fig. 3. Polaromechanical normal-mode splitting. **a** Frequency schematic diagram associated with the measurement. A red-detuned microwave field (red arrow) is used to drive the upper-branch polariton. The detuning is equal to the mechanical frequency, such that the scattered anti-Stokes mechanical sideband is in resonance with the polariton. **b** Output spectra of the polaromechanical normal modes for different drive powers, with $\Delta_{pd} = \omega_p - \omega_d$. The corresponding decay rates of the upper-branch polariton $\kappa_+/2\pi$ are 6.99, 0.25, 1.26, 1.45, 1.42, 1.50 and 0.45 kHz, respectively. We observe three adjacent mechanical modes and focus on the normal-mode splitting associated with the mode of frequency $\omega_b/2\pi = 10.9565$ MHz (see SI for more details). Black solid curves are fitting results. **c** The pump-enhanced effective polaromechanical coupling strength G_+ versus drive power. **d** Effective mechanical damping rate $\kappa_{b,\text{eff}}$ versus drive power.

cools the mechanical motion, yielding an increased mechanical damping rate [40].

In the first graph of Fig. 3b, a low drive power of -6.8 dBm leads to a weak coupling $G_+/2\pi = 3.06$ kHz, and the system is in the weak-coupling regime because $G_+ < \kappa_+ = 2\pi \times 6.99$ kHz. The anti-Stokes sideband is manifested as the magnomechanically induced transparency [38], and the mechanical damping rate is increased from $\kappa_b/2\pi = 155$ Hz to $\kappa_{b,\text{eff}}/2\pi = 250$ Hz. By further increasing the drive power, G_+ becomes greater than both κ_+ and $\kappa_{b,\text{eff}}$. For example in the second graph, $G_+/2\pi = 5.40$ kHz at the power of 2.4 dBm, which is greater than $\kappa_+/2\pi = 0.25$ kHz and $\kappa_{b,\text{eff}}/2\pi = 255$ Hz. The system then enters the *triple* strong-coupling regime. From the top to the bottom graph of Fig. 3b, as the power increases from -6.8 dBm to 16.53 dBm, the coupling G_+ gradually increases to 25.71 kHz (corresponding to a maximum polaromechanical cooperativity $C_{+,b} \equiv G_+^2/(\kappa_+\kappa_b) \approx 9.40 \times 10^3$), which exhibits a more evident feature of the NMS with the splitting of $2G_+$ in the spectra. Similar strong coupling induced NMS has been observed in cavity optomechanics [8–10]. Note that in Fig 3b, the frequency of the mechanical mode slightly decreases when increasing the power, which is

due to the magnon-phonon cross-Kerr effect [41] (see SI for more details). Figures 3c and 3d show the corresponding coupling strength G_+ and the effective mechanical damping rate $\kappa_{b,\text{eff}}$ for the drive powers used in Fig. 3b.

Another typical characteristics of the strong coupling is the anti-crossing, i.e., the level repulsion, in the frequency spectrum. In Fig. 4a, we fix the drive frequency at $\omega_d/2\pi = 7.205365$ GHz, and thereby the scattered mechanical sideband is at $\omega_d + \omega_b = 2\pi \times 7.216313$ GHz. By varying the drive power and utilizing the magnon self-Kerr effect, the frequency of the upper-branch polariton can be continuously adjusted. When the polariton frequency is approaching and then passing across the mechanical sideband, the normal-mode spectrum shows an anti-crossing feature due to the polaromechanical strong coupling. It is worth noting that the mechanical sideband is set at the CPA frequency ω_{CPA} , at which the polariton has the smallest decay rate. Figure 4b shows a significant enhancement of the polaromechanical cooperativity as the frequency of the upper-branch polariton approaches the CPA frequency.

Conclusion and discussion

We have demonstrated triple strong coupling in a polarome-

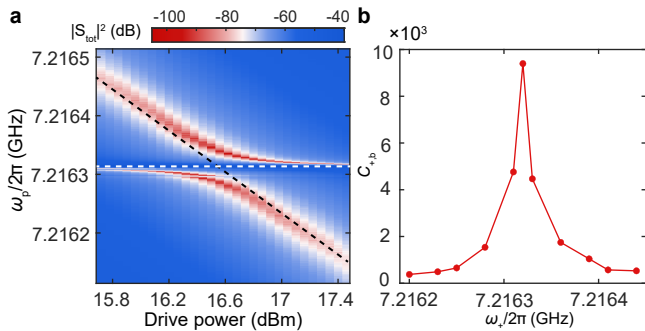


Fig. 4. Anti-crossing in the normal mode spectrum. **a** Output spectrum of the coupled upper-branch polariton and the mechanical mode versus the drive power. Due to the magnon self-Kerr effect, the frequency of the polariton shifts by increasing the drive power (black dashed line). The scattered mechanical sideband is fixed at 7.216313 GHz (white dashed line). **b** Polaromechanical cooperativity $C_{+,b}$ versus the frequency of the upper-branch polariton. The cooperativity gets significantly improved when the polariton resonates with the mechanical sideband at the CPA frequency.

chanical hybrid system, where the mechanical vibration mode is strongly coupled to the driven polariton, whose decay rate is significantly reduced via realizing the coherent perfect absorption. We have measured the corresponding normal-mode splitting at the mechanical sideband, and a high polaromechanical cooperativity $C_{+,b} = 9.40 \times 10^3$, which is *three orders of magnitude* higher than the previous experiments [38, 40, 41]. This will significantly boost the mechanical cooling efficiency and lower the threshold for achieving phonon lasers in cavity magnomechanics [40].

A quantum cooperativity $C_{+,b}^Q \equiv C_{+,b}/\bar{n}_b \gg 1$ (\bar{n}_b , the mean thermal phonon number) can be reached if placing the system at cryogenic temperatures. This would enable various quantum applications, e.g., the protocols for preparing macroscopic quantum states of magnons and phonons [39, 49, 50], which are useful in testing the limits of quantum mechanics, and quantum entangled or squeezed states of microwave fields [51, 52]. The triple strong coupling that we report here can act as a foundation for building multifunctional HQSs involving more different quanta, e.g., by coupling the microwave cavity to superconducting qubits [19] and the me-

chanical vibration to optical photons [47]. Our results can also be applied to YIG nano-structures [53] or planar configurations [54–56], which would enable the integration of magnonic devices on a chip and thus improve the functionality of the HQS to be used in quantum information processing or quantum sensing.

Methods

The magnonic system shows an excellent tunability in its resonance frequency. In this work, we utilize two methods to adjust the frequency of the magnon mode. One is to adjust the external bias magnetic field via $\omega_m = \gamma B_0$; the other is to use the magnon self-Kerr effect, reflected in the frequency of the driven magnon mode $\tilde{\omega}_m \approx \omega_m + 2K_m|M|^2$ (see SI for details). Both methods can achieve the same effect. When the strong drive field is absent, we alter the external bias magnetic field to adjust the magnon frequency, as done in Fig. 2a. When the drive field is applied, we alter the power of the drive field to change the magnon excitation number, which adjusts the magnon frequency due to the self-Kerr effect, as done in Fig. 4a.

In the experiment, we measure a negative self-Kerr coefficient $K_m/2\pi = -7.4$ nHz. The magnon mode experiences a negative frequency shift by increasing the drive power. To compensate for this effect, Fig. 3b is measured under different initial frequencies of the upper-branch polariton. From the top to the bottom graph, we increase the external magnetic field B_0 to have a higher initial magnon frequency (without applying the drive), and thus a higher initial frequency of the upper-branch polariton. This compensates the negative frequency shift of the magnon mode when the drive is applied, such that the anti-Stokes mechanical sideband is always kept in resonance with the polariton at different drive powers.

Data availability

The datasets used to generate the plots in the paper are available on Zenodo (<https://zenodo.org/records/12732420>). All other data that support the plots within this paper and other findings of this study are available from the corresponding authors upon reasonable request.

-
- [1] Xiang, Z.-L., Ashhab, S., You, J. Q. & Nori, F. Hybrid quantum circuits: Superconducting circuits interacting with other quantum systems. *Rev. Mod. Phys.* **85**, 623 (2013).
- [2] Kurizki, G. et al. Quantum technologies with hybrid systems. *Proc. Natl. Acad. Sci. U.S.A.* **112**, 3866 (2015).
- [3] Clerk, A. A., Lehnert, K. W., Bertet, P., Petta, J. R. & Nakamura, Y. Hybrid quantum systems with circuit quantum electrodynamics. *Nat. Phys.* **16**, 257 (2020).
- [4] Schleier-Smith, M. Editorial: Hybridizing Quantum Physics and Engineering. *Phys. Rev. Lett.* **117**, 100001 (2016).
- [5] Thompson, R. J., Rempe, G. & Kimble, H. J. Observation of normal-mode splitting for an atom in an optical cavity. *Phys. Rev. Lett.* **68**, 1132 (1992).
- [6] Wallraff, A. et al. Strong coupling of a single photon to a superconducting qubit using circuit quantum electrodynamics. *Nature* **431**, 162 (2004).
- [7] Weisbuch, C., Nishioka, M., Ishikawa, A. & Arakawa, Y. Observation of the coupled exciton-photon mode splitting in a semiconductor quantum microcavity. *Phys. Rev. Lett.* **69**, 3314 (1992).
- [8] Gröblacher, S., Hammerer, K., Vanner, M. R. & Aspelmeyer, M. Observation of strong coupling between a micromechanical resonator and an optical cavity field. *Nature* **460**, 724 (2009).
- [9] Teufel, J. D. et al. Circuit cavity electromechanics in the strong-coupling regime. *Nature* **471**, 204 (2011).
- [10] Verhagen, E., Deléglise, S., Weis, S., Schliesser, A. & Kippenberg, T. J. Quantum-coherent coupling of a mechanical oscillator to an optical cavity mode. *Nature* **482**, 63 (2012).

- [11] O’Connell, A. D. et al. Quantum ground state and single-phonon control of a mechanical resonator. *Nature* **464**, 697 (2010).
- [12] Chu, Y. et al. Quantum acoustics with superconducting qubits. *Science* **358**, 199 (2017).
- [13] Satzinger, K. J. et al. Quantum control of surface acoustic wave phonons. *Nature* **563**, 661 (2018).
- [14] Chu, Y. et al. Creation and control of multi-phonon Fock states in a bulk acoustic-wave resonator. *Nature* **563**, 666 (2018).
- [15] Mirhosseini, M., Sipahigil, A., Kalae, M. & Painter, O. Superconducting qubit to optical photon transduction. *Nature* **588**, 599 (2020).
- [16] Bennett, S. D., Cockins, L., Miyahara, Y., Grütter, P. & Clerk, A. A. Strong Electromechanical Coupling of an Atomic Force Microscope Cantilever to a Quantum Dot. *Phys. Rev. Lett.* **104**, 017203 (2010).
- [17] Karg, T. M. et al. Light-mediated strong coupling between a mechanical oscillator and atomic spins 1 meter apart. *Science* **369**, 174 (2020).
- [18] Schwab, K. C. & Roukes, M. L. Putting mechanics into quantum mechanics. *Phys. Today* **58**, 36 (2005).
- [19] Lachance-Quirion, D., Tabuchi, Y., Gloppe, A., Usami, K. & Nakamura, Y. Hybrid quantum systems based on magnonics. *Appl. Phys. Exp.* **12**, 070101 (2019).
- [20] Awschalom D. D. et al. Quantum engineering with hybrid magnonic systems and materials. *IEEE Trans. Quantum Eng.* **2**, 1 (2021).
- [21] Li, Y. et al. Hybrid magnonics: physics, circuits and applications for coherent information processing. *J. Appl. Phys.* **128**, 130902 (2020).
- [22] Li, J., Wang, Y.-P., Wu, W.-J., Zhu, S.-Y. & You, J. Q. Quantum Network with Magnonic and Mechanical Nodes. *PRX Quantum* **2**, 040344 (2021).
- [23] Chumak, A. V. et al. Advances in magnetics roadmap on spin-wave computing. *IEEE Trans. Magn.* **58**, 1 (2022).
- [24] Yuan, H. Y., Cao, Y., Kamra, A., Duine, R. A. & Yan, P. Quantum magnonics: When magnon spintronics meets quantum information science. *Phys. Rep.* **965**, 1 (2022).
- [25] Rameshti, B. Z. et al. Cavity magnonics. *Phys. Rep.* **979**, 1 (2022).
- [26] Pirro, P., Vasyuchka, V. I., Serga, A. A., & Hillebrands, B. Advances in coherent magnonics. *Nat. Rev. Mater.* **6**, 1114 (2021).
- [27] Santos, P. V. & Fainstein, A. Polaromechanics: polaritons meets optomechanics. *Opt. Mater. Exp.* **13**, 1974 (2023).
- [28] Basov, D. N., Asenjo-Garcia, A., Schuck, P. J., Zhu, X. & Rubio, A. Polariton panorama. *Nanophotonics* **10**, 549 (2021).
- [29] Chong, Y. D., Ge, L., Cao, H. & Stone, A. D. Coherent Perfect Absorbers: Time-Reversed Lasers. *Phys. Rev. Lett.* **105**, 053901 (2010).
- [30] Wan, W. et al. Time-Reversed Lasing and Interferometric Control of Absorption. *Science* **331**, 889 (2011).
- [31] Noh, H., Chong, Y. D., Stone, A. D. & Cao, H. Perfect coupling of light to surface plasmons by coherent absorption. *Phys. Rev. Lett.* **108**, 186805 (2012).
- [32] Wang, C., Sweeney, W. R., Stone, A. D. & Yang, L. Coherent perfect absorption at an exceptional point. *Science* **373**, 1261 (2021).
- [33] Zhang, D., Luo, X. Q., Wang, Y.-P., Li, T. F. & You, J. Q. Observation of the exceptional point in cavity magnon-polaritons. *Nat. Commun.* **8**, 1368 (2017).
- [34] Zuo, X. et al. Cavity magnomechanics: from classical to quantum. *New J. Phys.* **26**, 031201 (2024).
- [35] Huebl, H. et al. High Cooperativity in Coupled Microwave Resonator Ferrimagnetic Insulator Hybrids. *Phys. Rev. Lett.* **111**, 127003 (2013).
- [36] Tabuchi, Y. et al. Hybridizing ferromagnetic magnons and microwave photons in the quantum limit. *Phys. Rev. Lett.* **113**, 083603 (2014).
- [37] Zhang, X., Zou, C. L., Jiang, L. & Tang, H. X. Strongly coupled magnons and cavity microwave photons. *Phys. Rev. Lett.* **113**, 156401 (2014).
- [38] Zhang, X., Zou, C.-L., Jiang, L. & Tang, H. X. Cavity magnomechanics. *Sci. Adv.* **2**, e1501286 (2016).
- [39] Li, J., Zhu, S.-Y. & Agarwal, G. S. Magnon-Photon-Phonon Entanglement in Cavity Magnomechanics. *Phys. Rev. Lett.* **121**, 203601 (2018).
- [40] Potts, C. A., Varga, E., Bittencourt, V., Kusminskiy, S. V. & Davis, J. P. Dynamical backaction magnomechanics. *Phys. Rev. X* **11**, 031053 (2021).
- [41] Shen, R.-C., Li, J., Fan, Z.-Y., Wang, Y.-P. & You, J. Q. Mechanical Bistability in Kerr-modified Cavity Magnomechanics. *Phys. Rev. Lett.* **129**, 1123601 (2022).
- [42] Anderson, P. W. & Suhl, H. Instability in the motion of ferromagnets at high microwave power levels. *Phys. Rev.* **100**, 1788 (1955).
- [43] Gardiner, C. W. & Collett, M. J. Input and output in damped quantum systems: Quantum stochastic differential equations and the master equation. *Phys. Rev. A* **31**, 3761 (1985).
- [44] del Hougne, P., Yeo, K. B., Besnier, P. & Davy, M. On-demand coherent perfect absorption in complex scattering systems: Time delay divergence and enhanced sensitivity to perturbations. *Laser Photonics Rev.* **15**, 2000471 (2021).
- [45] Chen, L., Anlage, S. M. & Fyodorov, Y. V. Generalization of Wigner time delay to subunitary scattering systems. *Phys. Rev. E* **103**, L050203 (2021).
- [46] Aspelmeyer, M., Gröblacher, S., Hammerer, K. & Kiesel, N. Quantum optomechanics—throwing a glance. *J. Opt. Soc. Am. B* **27**, A189 (2010).
- [47] Aspelmeyer, M., Kippenberg, T. J. & Marquardt, F. Cavity optomechanics. *Rev. Mod. Phys.* **86**, 1391 (2014).
- [48] Wang, Y.-P. et al. Bistability of cavity magnon polaritons. *Phys. Rev. Lett.* **120**, 057202 (2018).
- [49] Li, J., Zhu, S.-Y. & Agarwal, G. S. Squeezed states of magnons and phonons in cavity magnomechanics. *Phys. Rev. A* **99**, 021801(R) (2019).
- [50] Li, J. & Zhu, S.-Y. Entangling two magnon modes via magnetostrictive interaction. *New J. Phys.* **21**, 085001 (2019).
- [51] Yu, M., Shen, H. & Li, J. Magnetostrictively Induced Stationary Entanglement between Two Microwave Fields. *Phys. Rev. Lett.* **124**, 213604 (2020).
- [52] Li, J., Wang, Y.-P., You, J. Q. & Zhu, S.-Y. Squeezing Microwaves by Magnetostriction. *Natl. Sci. Rev.* **10**, nwac247 (2023).
- [53] Heyroth, F. et al. Monocrystalline Freestanding Three-Dimensional Yttrium-Iron-Garnet Magnon Nanoresonators. *Phys. Rev. Appl.* **12**, 054031 (2019).
- [54] Xu, J. et al. Coherent Pulse Echo in Hybrid Magnonics with Multimode Phonons. *Phys. Rev. Appl.* **16**, 024009 (2021).
- [55] Li, Y. et al. Strong Coupling between Magnons and Microwave Photons in On-Chip Ferromagnet-Superconductor Thin-Film Devices. *Phys. Rev. Lett.* **123**, 107701 (2019).
- [56] Hatanaka, D. et al. On-Chip Coherent Transduction between Magnons and Acoustic Phonons in Cavity Magnomechanics. *Phys. Rev. Appl.* **17**, 034024 (2022).

Acknowledgments

The authors thank Liu Qiu and Yanhao Tang for useful discussions. This work was supported by National Key

Research and Development Program of China (Grant No. 2022YFA1405200) and National Natural Science Foundation of China (Grant Nos. 92265202, 11934010, 12174329), and the Fundamental Research Funds for the Central Universities (No. 2021FZZX001-02).

Author contributions

R.C.S. performed the measurements and R.C.S. and X.Z. developed the theory. The measurement and theory related to the polariton-mechanics coupling is under the supervision

of J.L. Y.M.S. and W.J.W. provided experimental support. R.C.S., J.L., Y.P.W. and J.Q.Y. analyzed the data. R.C.S., J.L. and J.Q.Y. wrote the manuscript with the input and comment from all co-authors. J.Q.Y. supervised the project.

Competing interests

The authors declare no competing interests.

Additional information

Supplementary information The online version contains supplementary material available at